Gate-tunable Kondo resistivity and dephasing rate in graphene studied by numerical renormalization group calculations

Po-Wei Lo,[1] Guang-Yu Guo,[1,2,*] and Frithjof B. Anders[3]

[1]*Department of Physics and Center for Theoretical Sciences, National Taiwan University, Taipei 10617, Taiwan*

[2]*Graduate Institute of Applied Physics, National Chengchi University, Taipei 11605, Taiwan*

[3]*Lehrstuhl für Theoretische Physik II, Technische Universität at Dortmund, DE-44221 Dortmund, Germany*

(Received 21 January 2014; revised manuscript received 7 April 2014; published 19 May 2014)

Motivated by the recent observation of the Kondo effect in graphene in transport experiments, we investigate the resistivity and dephasing rate in the Kondo regime due to magnetic impurities in graphene with different chemical potentials (μ). The Kondo effect due to either carbon vacancies or magnetic adatoms in graphene is described by the single-orbital pseudogap asymmetric Anderson impurity model which is solved by the accurate numerical renormalization group method. We find that although the Anderson impurity model considered here is a mixed-valence system, it can be driven into either the Kondo [$\mu > \mu_c$ (critical value) > 0], mixed-valency ($\mu \approx \mu_c$), or empty-orbital ($\mu < \mu_c$) regime by a gate voltage, giving rise to characteristic features in resistivity and dephasing rate in each regime. Specifically, in the case of $\mu < \mu_c$, the shapes of the resistivity (dephasing rate) curves for different μ are nearly identical. However, as temperature decreases, they start to increase to their maxima at a lower T/T_K, but more rapidly [as $(T_K/T)^{3/2}$] than in normal metals [here, T (T_K) denotes the (Kondo) temperature]. As T further decreases, after reaching the maximum, the dephasing rate drops more quickly than in normal metals, behaving as $(T/T_K)^3$ instead of $(T/T_K)^2$. Furthermore, the resistivity has a distinct peak above the saturation value near T_K. In the case of $\mu > \mu_c$, in contrast, the resistivity curve has an additional broad shoulder above $10T_K$ and the dephasing rate exhibits an interesting shoulder-peak shape. In the narrow boundary region ($\mu \approx \mu_c$), both the resistivity and dephasing rate curves are similar to the corresponding ones in normal metals. This explains the conventional Kondo-like resistivity from recent experiments on graphene with defects, although the distinct features in the resistivity in the other cases ($\mu < \mu_c$ or $\mu > \mu_c$) were not seen in the experiments. The interesting features in the resistivity and dephasing rate are analyzed in terms of the calculated T-dependent spectral function, correlation self-energy, and renormalized impurity level.

DOI: 10.1103/PhysRevB.89.195424 PACS number(s): 72.10.Fk, 72.15.Qm, 72.80.Vp, 73.22.Pr

I. INTRODUCTION

Interactions between particles in many-body systems are responsible for the formation of correlated many-body states which lead to a plethora of quantum phenomena. Therefore, the many-body correlation in quantum systems has been one of the most significant topics in condensed-matter physics. Graphene, a newly discovered two-dimensional material with carbon atoms arranged in a single-layer honeycomb lattice possessing an unusual band structure with a linear spectrum, hosts two-dimensional Dirac fermions [1–3]. It provides a great opportunity to investigate novel many-body correlation in low-dimensional Dirac fermion systems. Furthermore, the easy manipulation of the Fermi level by an applied gate voltage also makes graphene an excellent candidate for important technological applications.

In particular, there has been an increasing interest in low-temperature behaviors of dilute magnetic impurities in graphene in recent years [4]. Local magnetic moments in graphene can be created by placing magnetic atoms onto the graphene sheet or by introducing point defects in the graphene sheet [5–11]. The theoretical model for describing the interactions of local magnetic moments with conduction electrons in metals was first formulated by Anderson, known as the Anderson impurity model [12]. The impurity and conduction electrons could form an entangled many-body state below the Kondo temperature (T_K) in the presence of the hybridizations between them. The magnetic moment of the impurity would then be screened by the formation of the many-body singlet, known as the Kondo effect [13]. However, in systems with a pseudogap, such as graphene, the Kondo effect could be significantly different [14–20]. For example, with vanishing density of state at the Fermi level, the tendency toward the screened impurity in graphene would get reduced. Therefore, the Kondo effect would only take place when the strength of the coupling of the impurity state to the conduction electrons (Γ_0) exceeds a critical value (Γ_c), resulting in an unusual phase diagram for the system. Up to now, the thermodynamical properties of graphene Kondo systems have been extensively studied [4,18,21].

However, the thermodynamical properties in graphene with dilute impurities are difficult to probe. On the other hand, transport properties are easier to measure. Indeed, resistivity evidence for the Kondo effect in graphene with vacancies has been recently reported [22]. By the manipulation of the Fermi level by an applied gate voltage, the carrier density becomes controllable. This provides a rare opportunity to study the carrier density tuning of the Kondo effect, which could lead to many interesting transport phenomena [22–27]. Under an applied gate voltage, for example, the Fermi level would move away from the Dirac point, and the density of states at the Fermi level becomes finite. Therefore, the magnetic moment of the impurity can be screened in the low-temperature

*gyguo@phys.ntu.edu.tw

limit. Although the thermodynamical properties of the system might become similar to that of normal metals, the impurity spectral function could have unusual characteristics [24,25]. These unusual characteristics would make the behaviors of the transport properties, such as resistivity and dephasing rate, become different from that of the conventional Kondo effect.

So far, however, there have been few studies on the transport properties in graphene with the Kondo effect [24,25] and all of these studies are on the tunneling spectra for scanning tunneling spectroscopy. In Ref. [24], the Anderson impurity model with the on-site Coulomb interaction $U \to \infty$ was solved within the slave-boson mean-field approximation, whereas in Ref. [25], the standard spin-1/2 Kondo model was treated using the nonperturbative numerical renormalization group (NRG) method [28]. In this work, we systematically study the behaviors of resistivity and dephasing rate in the Kondo regime in the asymmetric Anderson impurity model with the realistic model parameters for graphene with carbon vacancies or magnetic adatoms. We use the accurate NRG method [28]. We find that although the asymmetric Anderson impurity model considered here is a mixed-valence system, it can be driven into either the Kondo, mixed-valency, or empty-orbital regime by a gate voltage, giving rise to characteristic features in resistivity and dephasing rate in each regime. The results not only explain the Kondo resistivity observed in recent experiments [22], but also suggest directions for further transport experiments to identify the exotic features of the Kondo effect in graphene. This rest of this paper begins with an introduction to the structure of graphene with local magnetic moments in Sec. II. This will be followed by a brief description of the Anderson impurity model for graphene with carbon vacancies and magnetic adatoms, and the NRG method in Sec. II. Then, the calculated resistivity and dephasing rate are presented in Sec. III. Recent experiments on the Kondo effect in graphene are discussed and further experiments on transport properties are suggested in Sec. IV. Finally, the conclusions that could be drawn from this work are given in Sec. V.

II. THEORY AND COMPUTATIONAL METHOD

A. The Anderson impurity model

The positions of impurities play an important role in the Kondo physics in graphene. Possible absorption sites on a graphene sheet can be classified as the top, hollow, and bridge ones. The systems with adatoms absorbed on the hollow and bridge sites are the candidates to realize the multichannel Kondo problem [29]. Other possible structures include carbon vacancies and substitutional impurities [21,30]. Nevertheless, in the systems with magnetic adatoms absorbed on the hollow and bridge sites and also substitutional impurities, the scattering rate is proportional to $|\omega+\mu|^3$, where ω and μ are the energy and chemical potential, respectively. This suggests that the Kondo effect would hardly occur in these systems [29,30]. In this paper, therefore, we consider only the cases of carbon vacancies and also magnetic adatoms absorbed on the top sites, which are the single-channel Kondo problems.

The Anderson impurity model can be written as [21,29]

$$\begin{aligned} H = &\sum_\sigma \epsilon_d f_\sigma^\dagger f_\sigma + U f_\uparrow^\dagger f_\uparrow f_\downarrow^\dagger f_\downarrow \\ &+ \sum_\sigma \int_{-D}^{D} d\omega |\omega+\mu| g_\sigma(\omega) c_\sigma^\dagger(\omega) c_\sigma(\omega) \\ &+ \sum_\sigma \int_{-D}^{D} d\omega \sqrt{\frac{\Gamma(\omega)}{\pi D}} [f_\sigma^\dagger c_\sigma(\omega) + c_\sigma^\dagger(\omega) f_\sigma], \end{aligned} \quad (1)$$

where $\sigma = \uparrow,\downarrow$; ϵ_d is the energy of the impurity level, and U is the Coulomb interaction between the electrons; $f_\uparrow^\dagger$ ($f_\downarrow^\dagger$) and $f_\uparrow$ ($f_\downarrow$) are creation and annihilation operators for an electron in the $\uparrow$ ($\downarrow$) impurity state; $c_\uparrow^\dagger(\omega)$ [$c_\downarrow^\dagger(\omega)$] and $c_\uparrow(\omega)$ [$c_\downarrow(\omega)$] are creation and annihilation operators for an electron in the $\uparrow$ ($\downarrow$) conduction states with energy equal to ω; and $g_\sigma(\omega)$ is the part of the density of states that couples to the impurity state. D is the total bandwidth. $\Gamma(\omega)$ is the scattering rate and related to $g_\sigma(\omega)$ by $\Gamma(\omega) = \pi g_\sigma(\omega)|V_{\rm hyb}(\omega)|^2$, where $V_{\rm hyb}(\omega)$ is the effective hybridization strength.

In the case of carbon vacancies, the scattering rate $\Gamma(\omega)$ can be written as [21]

$$\Gamma^{(\rm vac)}(\omega) = \frac{\Omega_0 V_{\rm vac}^2 |\omega+\mu|}{2\hbar^2 v_F^2}\left[2 - J_0\left(\frac{2}{3}\frac{|\omega+\mu|}{t}\right)\right], \quad (2)$$

where Ω_0, v_F, t, and $V_{\rm vac}$ are the unit cell area, the Fermi velocity, the hopping energy, and the hybridization strength, respectively; J_0 is the zeroth Bessel function. Since we only consider the cases of small chemical potentials, the value of $(2/3)(|\omega+\mu|/t)$ is small for small ω. Therefore, we can expand J_0 at $\omega = 0$, and $\Gamma^{(\rm vac)}(\omega)$ can be approximated as

$$\Gamma^{(\rm vac)}(\omega) = \frac{\Omega_0 V_{\rm vac}^2 |\omega+\mu|}{2\hbar^2 v_F^2}\left[1 + \frac{4}{27}\left(\frac{|\omega+\mu|}{t}\right)^2\right]. \quad (3)$$

Hence the effective hybridization strength can be written as

$$V_{\rm hyb}^{(\rm vac)}(\omega) = V_{\rm vac}\sqrt{1 + \frac{4}{27}\left(\frac{|\omega+\mu|}{t}\right)^2}. \quad (4)$$

In the case of adatoms on the top sites, the tight-binding formalism is used. We only need to consider the hybridizations of the impurity with the conduction electrons below the impurity and the next-nearest neighbors. Thus, the scattering rate can be written as [29]

$$\Gamma^{(\rm ada)}(\omega) = \frac{\Omega_0 V_A^2 |\omega+\mu|}{2\hbar^2 v_F^2}\left[1 - \frac{(\omega+\mu)}{t}\frac{V_B}{V_A}\right]^2, \quad (5)$$

where V_A is the hybridization of the impurity with the conduction electron below the impurity, and V_B is the hybridization of the impurity with the conduction electrons on the next-nearest neighbors. In general, $V_B \ll V_A$. The effective hybridization strength can be approximated as

$$V_{\rm hyb}^{(\rm ada)}(\omega) = V_A\left[1 - \frac{(\omega+\mu)}{t}\frac{V_B}{V_A}\right]. \quad (6)$$

In this work, therefore, the following scattering rate is assumed:

$$\Gamma(\omega) = \begin{cases} \Gamma_0|\tilde{\omega}+\tilde{\mu}|s(\tilde{\omega}+\tilde{\mu}), & |\tilde{\omega}+\tilde{\mu}| \leqslant 1 \\ \Gamma_0 s\left(\frac{\tilde{\omega}+\tilde{\mu}}{|\tilde{\omega}+\tilde{\mu}|}\right), & 1 < |\tilde{\omega}+\tilde{\mu}|, |\tilde{\omega}| \leqslant \frac{D}{D_{\rm eff}} \\ 0, & |\tilde{\omega}| > \frac{D}{D_{\rm eff}}, \end{cases}$$

where $\Gamma_0 = \Omega_0 V^2 D_{\rm eff}/2\hbar^2 v_F^2$; $V = V_{\rm vac}$ (V_A) for the case of carbon vacancies (adatoms); $\tilde{\omega} = \omega/D_{\rm eff}$ and $\tilde{\mu} = \mu/D_{\rm eff}$; $D_{\rm eff}$ is the effective bandwidth within which the density of states is approximately proportional to $|\omega+\mu|$; and $s(x)$ is defined as

$$s(x) = \begin{cases} 1+\alpha x^2 & \text{for carbon vacancies} \\ (1-\beta x)^2 & \text{for adatoms,} \end{cases}$$

where $\alpha = (4/27)(D_{\rm eff}/t)^2$ and $\beta = (D_{\rm eff}/t)(V_B/V_A)$.

In this work, we exploit the powerful NRG method [28] to solve the Anderson impurity model. In all of the present calculations, we use the discretization parameter $\Lambda = 1.8$ and keep 1200 states per NRG iteration so that the obtained resistivity and dephasing rate converge within 0.1%. The valence bandwidth of the graphene band structure is about 20 eV and the linear dispersion extends up to about 2 eV above and below the Dirac point [6]. Therefore, we set $D = 20$ eV and $D_{\rm eff} = 2$ eV. Test NRG calculations with different D values show that the calculated thermodynamic and transport properties are unaffected by the particular D value used. Parameters ϵ_d, U, and Γ_0 (V) would depend on the type of impurities. Typically, U varies from about 1 to 10 eV, Γ_0 of the order of 1 eV, and ϵ_d is around -1 eV [5–9,21,25]. We have explored a wide parameter range. The calculated thermal properties such as susceptibility, entropy, Kondo temperature, and specific heat are consistent with previous theoretical reports [18,21,24,25]. In this paper, we use parameters $U = 10$ eV, $\epsilon_d = -0.7$ eV, and $\Gamma_0 = 1$ eV (i.e., $V = 2.6$ eV). That is, we consider a mixed-valence system since $|\epsilon_d|/\Gamma_0 \leqslant 1$ [31,32]. Interestingly, as will be demonstrated below, this mixed-valence graphene system can be driven into either the Kondo, mixed-valency, or empty-orbital regime by a gate voltage, giving rise to contrasting behaviors in resistivity and dephasing rate.

B. Resistivity calculation

To obtain resistivity and dephasing rate, we first calculate the temperature (T)-dependent single-particle Green's function $G_\sigma^f(\omega,T)$ of the impurity by the NRG method [28]. The impurity spectral function is defined as $A_\sigma^f(\omega,T) = -(1/\pi)\mathrm{Im}G_\sigma^f(\omega,T)$ and can be calculated directly by the Lehmann representation,

$$A_\sigma^f(\omega,T) = \frac{1}{Z(T)}\sum_{r,r'}|M_{r,r'}|^2(e^{E_r/k_BT}+e^{E_r'/k_BT}) \times \delta[\omega-(E_r'-E_r)], \quad (7)$$

where $Z(T)$ is the partition function and $M_{r,r'} = \langle r|f_\sigma|r'\rangle$ is the relevant many-body matrix element; $|r\rangle$ ($|r'\rangle$) is the many-body eigenstate and E_r (E_r') is the corresponding eigenenergy. The real part of $G_\sigma^f(\omega,T)$ can be obtained via Kramers-Kronig relation. In the present calculations, the method for improving the resolution of $A_\sigma^f(\omega,T)$ is used [33].

Single-particle Green's function $G_\sigma(\omega,T)$ for the conduction electrons can be written as [13]

$$G_\sigma(\omega,T) = G_\sigma^0(\omega,T) + G_\sigma^0(\omega,T)c_{\rm imp}T_\sigma(\omega,T)G_\sigma^0(\omega,T), \quad (8)$$

where $G_\sigma^0(\omega,T)$ is the single-particle Green's function for the noninteracting conduction electrons. The single impurity T matrix $T_\sigma(\omega,T)$ is given by $|V_{\rm hyb}(\omega)|^2G_\sigma^f(\omega,T)$ [13]. For a small impurity concentration $c_{\rm imp}$, $G_\sigma(\omega,T)$ is determined by the Dyson equation,

$$G_\sigma(\omega,T) = G_\sigma^0(\omega,T) + G_\sigma^0(\omega,T)c_{\rm imp}T_\sigma(\omega,T)G_\sigma(\omega,T), \quad (9)$$

which is valid to the first order of $c_{\rm imp}$. In this approximation, the self-energy $\Sigma_\sigma(\omega,T)$ for the conduction electrons is equal to $c_{\rm imp}T_\sigma(\omega,T)$. Then, the relaxation time can be obtained by taking the imaginary part of $\Sigma_\sigma(\omega,T)$. By substituting $A_\sigma^f(\omega,T)$ for $T_\sigma(\omega,T)$, the expression of the relaxation time can be written as

$$\frac{1}{\tau_\sigma(\omega,T)} = \frac{2\pi c_{\rm imp}|V_{\rm hyb}(\omega)|^2}{\hbar}A_\sigma^f(\omega,T). \quad (10)$$

Finally, based on the Boltzmann transport theory and using $\tau_\sigma(\omega,T)$ obtained above, the resistivity (sum over two spin) can be written in the form

$$\rho_m(T) = \rho_0\left\{\int\left[-\frac{\partial f(\omega)}{\partial\omega}\right]\frac{|\omega+\mu|d\omega}{|V_{\rm hyb}(\omega)|^2A_\sigma^f(\omega,T)}\right\}^{-1}, \quad (11)$$

where $\rho_0 = 4\pi^2c_{\rm imp}\hbar/e^2$ and $f(\omega)$ is the Fermi-Dirac distribution function.

C. Dephasing rate calculation

An electron could interact with another electron through an inelastic-scattering event. This scattering would change its energy and hence the evolution of its phase. Consequently, the phase of the electron wave would suffer some dephasing. Therefore, the dephasing rate can be defined as the inelastic-scattering rate. The total scattering rate has already been given in Eq. (10). The elastic-scattering rate can be derived from the Fermi golden rule, and written as

$$\frac{1}{\tau_\sigma^{(\rm ela)}(\omega,T)} = \frac{2c_{\rm imp}|V_{\rm hyb}(\omega)|^2}{\hbar}\Gamma(\omega)\left|G_\sigma^f(\omega,T)\right|^2. \quad (12)$$

Finally, the dephasing rate can be obtained as the difference between the total scattering rate and the elastic scattering. Therefore, the ω-resolved dephasing rate can be written as [34]

$$\frac{1}{\tau_\sigma^\phi(\omega,T)} = \frac{2c_{\rm imp}|V_{\rm hyb}(\omega)|^2}{\hbar} \times\left[\pi A_\sigma^f(\omega,T) - \Gamma(\omega)\left|G_\sigma^f(\omega,T)\right|^2\right]. \quad (13)$$

In experiments, measurement of the resistivity correction to the weak-localization effect can be used to determine the dephasing rate [35]. To compare to experiments, one should calculate the total dephasing rate $\gamma_m(T)$, which for

two-dimensional structures is given by an integral over the ω-resolved dephasing rate as [36]

$$\gamma_m^{\phi}(T) = \frac{1}{\tau}\exp\left\{\int\left[-\frac{\partial f(\omega)}{\partial\omega}\right]\ln\frac{\tau}{\tau_\sigma^{\phi}(\omega,T)}d\omega\right\}, \quad (14)$$

where τ is the unit time.

III. RESULTS AND DISCUSSION

Before presenting the calculated transport properties, let us first examine the phase diagram of the Kondo effect in graphene. In pure graphene (i.e., $\mu = 0$), there are two stable fixed points, i.e., the local-moment (LM) and frozen-impurity (FI) fixed points [31]. The system would flow to either the LM or FI regime in the low-temperature limit, depending critically on the Γ_0 value. When the Fermi level is slightly raised or lowered, however, the LM fixed point will become unstable. Also, there will be another stable fixed point, namely, the strong-coupling (SC) fixed point, when μ is positive. Nevertheless, although the system where Γ_0 is smaller than the critical value could enter the SC regime [31], T_K could be very low [25], which would not be experimentally accessible. Therefore, we only investigate the cases where Γ_0 is larger than the critical value ($\Gamma_c = 0.953$ eV).

Note that in the recent literature [4,21,25,27], the FI and SC fixed points are generally referred to as the asymmetric SC point. We believe that this is, at a minimum, not precise since, as we demonstrate below, the spectral function and transport properties are quite different in the FI and SC regimes. Therefore, here we consider the FI and SC fixed points (regimes) as two different fixed points (regimes). Nevertheless, in this paper, for simplicity, we loosely use the Kondo temperature T_K to denote the temperature where the system would enter either the SC or FI regime from either the LM or VF regime. Strictly speaking, one should use another symbol (e.g., T^*) to denote the transition from the VF to FI regime since there is no Kondo effect in this crossover.

Figure 1 shows the dependence of the Kondo temperature and also the impurity state occupation number (n) on the chemical potential. Here, T_K is defined by $S_{\rm imp}/k_B = (1/2)\ln 2$, where $S_{\rm imp}$ is the impurity entropy and k_B is the Boltzmann constant, respectively. It is clear that there is a pronounced particle-hole asymmetry in the graphene Kondo systems [25]. As mentioned in Sec. II A, the graphene Kondo systems with the types of impurities we consider here are a mixed-valence system. Therefore, as one might expect from the conventional Anderson impurity model, there is no LM fixed point and only one crossover, namely, the crossover from the valence-fluctuation (VF) to FI regime [31] for the negative μ values, as shown in Fig. 1(a). When the Fermi level is lowered below the Dirac point, the density of states at the Fermi level increases and so does the scattering rate. Therefore, T_K increases with $|\mu|$ [Fig. 1(a)]. In the positive μ case, in contrast, T_K initially decreases with $|\mu|$ and then reaches a minimum near $\mu = \mu_m = \sim 0.04$ eV. As the Fermi level is further raised, T_K increases monotonically with $|\mu|$. We could attribute this interesting behavior to the occurrence of the LM fixed point when $\mu > \mu_c = 0.0126$ eV, which is also evident from the sharp increase of the occupation number of the impurity state around $\mu \approx \mu_c$ [see the inset in Fig. 1(a)].

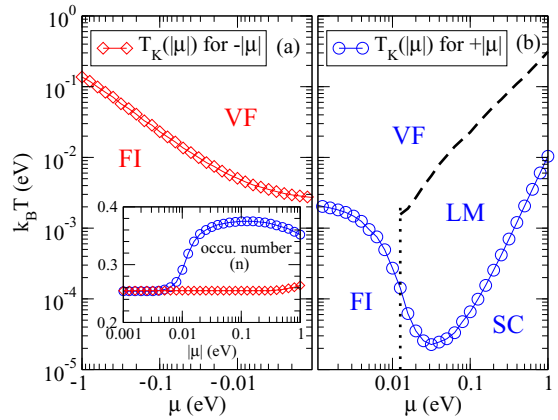

FIG. 1. (Color online) Kondo temperature T_K as a function of chemical potential μ. T_K is defined by $S_{\rm imp}/k_B = (1/2)\ln 2$. VF: valence-fluctuation regime; LM: local-moment regime; FI: frozen-impurity regime; SC: strong-coupling regime. (a) The zero-temperature occupation number (n) of the impurity spin-up (spin-down) state is displayed as a function of the magnitude of chemical potential ($|\mu|$) in the inset. (b) The dashed line, determined by $S_{\rm imp}/k_B = 1.2\ln 2$, indicates the approximate boundary between the VF and LM regimes; the vertical dot line at $\mu = \mu_c = 0.0126$ eV indicates the approximate boundary between the FI and SC regimes (see Sec. III C). The minimal T_K occurs at $\mu = \mu_m = \sim 0.04$ eV.

Therefore, the system would enter the SC regime at lower temperatures from the LM regime (i.e., the Kondo effect) rather than the VF regime [Fig. 1(b)]. Interestingly, in the SC regime ($\mu > \mu_C$), the rise of the Kondo temperature with μ for $\mu > \mu_m$ can be fitted by relation $k_B T_K \approx 0.01\mu^{2.2}$. The exponent is slightly smaller than that (2.6) in Ref. [25], in which the Kondo model is considered.

It is reported in Ref. [37] that due to the unique electron-phonon interaction, the electronic density of states near the Dirac point in graphene would be renormalized when $|\mu| > 0.2$ eV. In particular, the density of states at the Dirac point would become finite and the density of states in the vicinity of this point would becomes quadratic rather than linear [37]. Nevertheless, the Kondo scale ($k_B T_K$) of the system considered in this paper is $\sim 10^{-5}$–10^{-1} eV (Fig. 1). As a result, even when the Dirac point is far away from the Fermi level ($|\mu| > 0.2$ eV), the finite density of states at the Dirac point and also its quadratic ω dependence will have no significant impact on the behaviors of the Kondo effect in graphene, as demonstrated by our NRG calculations for $\mu = \pm 0.5$ eV. Therefore, throughout this paper, we neglect this effect of the electron-phonon interaction and thus treat the density of states as being linear in the energy range of $|\omega + \mu| \leqslant D_{\rm eff}$.

A. Resistivity versus temperature

Figure 2 shows the T dependence of the resistivity and also the spectral function at $T = 0$ under different chemical potentials. In the present calculations, we first set $s(x) = 1$, and the scattering rate becomes the power law of $r = 1$. This means that for the case of carbon vacancies, the higher-order terms in the scattering rate are neglected, and that for the case of adatoms only the hybridization of the impurity with conduction

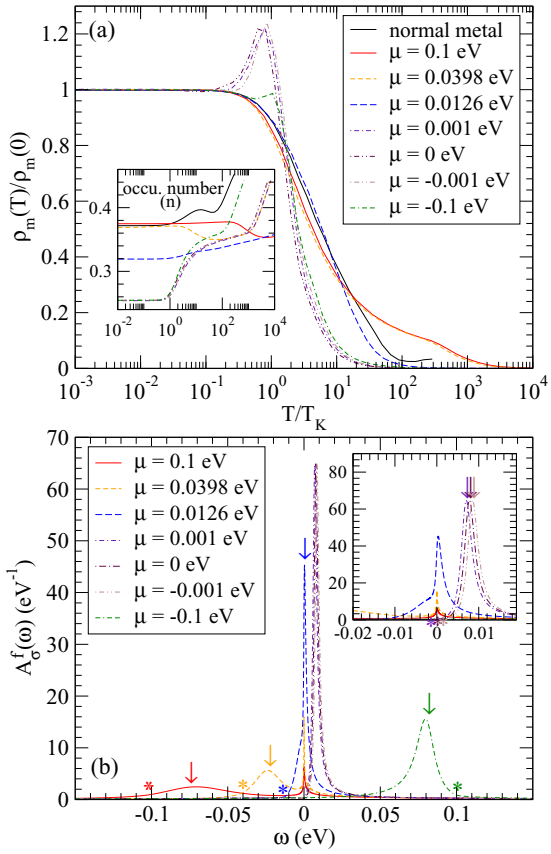

FIG. 2. (Color online) (a) Resistivity as a function of temperature for different chemical potentials. Inset: Occupation number (n) of the impurity spin-up (spin-down) state as a function of temperature for different chemical potentials. (b) Impurity spectral function at zero temperature under different chemical potentials μ. $\omega = 0$ is the Fermi level. The stars indicate the positions of the Dirac point; the arrows denote the positions of the effective (renormalized) impurity level ($\tilde{\epsilon_d}$).

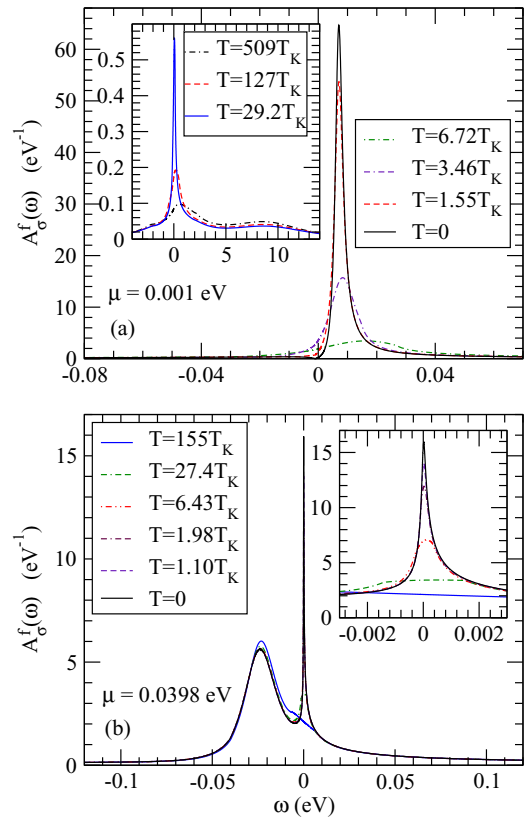

FIG. 3. (Color online) Impurity spectral function for (a) $\mu = 0.001$ eV and (b) $\mu = 0.0398$ eV at different temperatures. $\omega = 0$ is the Fermi level.

electrons below the impurity is considered. In general, all the resistivity-versus-T curves in the graphene Kondo systems, especially that for $\mu = 0.0126$ eV, look similar to that of the usual Kondo effect [38]. As the systems go through the crossover region from the high-T VF regime to low-T FI (or SC) regime, the resistivity increases steeply and eventually saturates to the zero-temperature resistivity [$\rho_m(0)$] near T_K.

Nevertheless, a closer examination of Fig. 2(a) shows that many resistivity-versus-T curves exhibit certain prominent features that are distinctly different from that in normal metals. In particular, the resistivity-versus-T curves can be grouped into three cases, depending on their chemical potentials [Fig. 2(a)]. The first case includes the systems with negative μ and also very small $|\mu|$ (e.g., $\mu = 0$ and ± 0.001 eV) values. The resistivity curves in this case have a pronounced peak near T_K, especially for very small $|\mu|$ values. When the temperature is lowered from about $100T_K$, the resistivity first rises rapidly to that above $\rho_m(0)$, but then drops quickly to $\rho_m(0)$ as temperature further decreases. This interesting feature is caused by the fact that the resonance of the impurity state is located at about 10 meV above the Fermi level [see the inset in Fig. 2(b)]. Therefore, as temperature decreases, the resonance peak becomes narrower and thus moves away from the Fermi level [see the inset in Fig. 3(a)]. Furthermore, as μ becomes more negative, the peak moves further above the Fermi level [see, e.g., the curve for $\mu = -0.1$ eV in Fig. 2(b)] and, consequently, the pronounced peak near T_K is reduced. Interestingly, there is no Kondo resonance at the Fermi level in the impurity spectral function at low temperatures in this case [see, e.g., Fig. 3(a)]. Therefore, the systems are driven from the high-T VF regime to the low-T FI regime rather than the SC regime. Interestingly, Fig. 2(a) shows that in the crossover from the VF to the FI regime, the resistivity curves in this case approach their saturation value in the same manner. However, the increase of the resistivity as the temperature decreases is much more rapid [as $1.68(T_K/T)^{3/2}$, as determined by a fitting to the resistivity curves] than that in the conventional Kondo effect [Fig. 2(a)].

The case of large positive μ values ($\mu > 0.0126$ eV) belongs to the second one. A common feature in this case is that apart from the resonance peak due to the impurity state, the sharp Kondo resonance appears at the Fermi level in the spectral function [see, e.g., the curves for $\mu = 0.0398$ and 0.10 eV in Fig. 2(b)]. As a result, the resistivity curve can be divided into two parts. The first part, with $T \geqslant 10T_K$, is mainly caused by the scattering of the local moment. The other part, with $T < 10T_K$, is due to the strong coupling between the impurity spin and conduction electrons. Figure 3(b) shows

that in the spectral function for $\mu = 0.0398$ eV, a wide peak centered at the effective impurity level $\tilde{\epsilon}_d = -0.021$ eV (also the Dirac point) and extended across the Fermi level forms at high temperatures. The sharp Kondo resonance at the Fermi level shows up as the temperature further decreases. The scattering of the local moment gives rise to the broad resistivity shoulder above $10T_K$ [Fig. 2(a)]. The Kondo resonance then causes the resistivity to rapidly rise, like the usual Kondo effect, as the system enters the SC regime. This interesting shoulder-peak feature can be attributed to the occurrence of the additional LM fixed point [Fig. 1(b)], as already discussed in the beginning of this section.

The third case includes the systems with a positive μ being close to $\mu = 0.0126$ eV. In this case, the impurity state peak is located at the Fermi level [Fig. 2(b)] and hence is merged with the Kondo resonance. There is no broad resistivity shoulder above $10T_K$. The resistivity curves look almost identical to that of conventional Kondo systems [Fig. 2(a)].

An interesting finding of this work is that for $\mu < \mu_c$, the system would be in the FI regime rather than the SC regime when $T < T_K$ (Fig. 1). In this FI regime, the spectral function would have only one peak located at the effective impurity level above the Fermi level [Figs. 2(b) and 3(a)]. In contrast, in the SC regime ($\mu > \mu_c$), the spectral function would have two peaks: one sitting on the Fermi level and the other located at the effective impurity level below the Fermi level [Figs. 2(b) and 3(b)]. Since the effective impurity level is above the Fermi level, the low-energy configuration of the impurity in the FI regime would be a nearly empty state [see the inset in Fig. 1(a)] and, therefore, there would be almost no local magnetic moment. This is quite different from that in the SC regime, where the local magnetic moment would be screened due to the formation of the spin singlet state with the conduction electrons.

B. Renormalization of the impurity level

In general, the impurity level in the Anderson model would be renormalized due to the Coulomb correlations [33]. As a result, the effective impurity level $\tilde{\epsilon}_d$ in the pure graphene would be shifted towards the Fermi level. The $U/|\epsilon_d|$ ratio and the Γ_0 value would determine whether the $\tilde{\epsilon}_d$ is below or above the Fermi level. With Γ_0 being smaller than the critical value Γ_c, $\tilde{\epsilon}_d$ would be located below the Fermi level. The system would flow to the LM regime in this case. Furthermore, since the density of states at the Fermi level is zero, the impurity magnetic moment could not be completely screened. Consequently, the system would stay in the LM regime at low temperatures. However, in the asymmetric Anderson model ($U \neq 2|\epsilon_d|$) with $\Gamma_0 > \Gamma_c$, $\tilde{\epsilon}_d$ would be located above the Fermi level, and the system would flow to the FI regime.

To evaluate the effective impurity level and also to see how the position of the resonant peak (ϵ_r) in the impurity spectral function evolves as temperature varies, let us rewrite the impurity Green's function as

$$G^f_\sigma(\omega,T) = \frac{1}{(\omega + i\delta) - \epsilon_d - \Sigma^U_\sigma(\omega,T) - \Delta_\sigma(\omega)}, \quad (15)$$

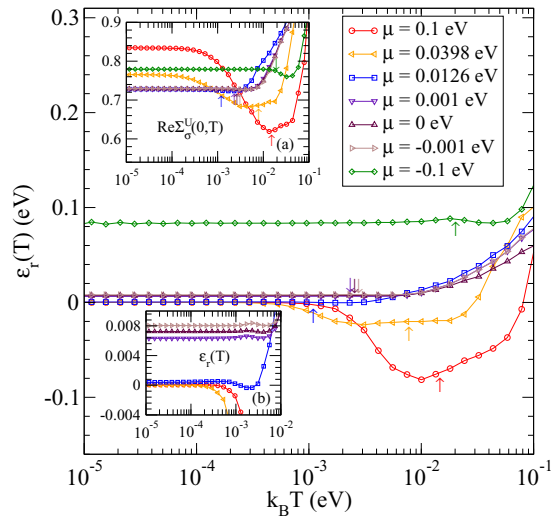

FIG. 4. (Color online) The energy of the resonant peak [$\epsilon_r(T)$] in the impurity spectral function for different chemical potentials as a function of temperature. The real part of the self-energy due to the Coulomb correlations [$\mathrm{Re}\Sigma^U_\sigma(0,T)$] for different chemical potential as a function of temperature is displayed in the inset of (a). The arrows indicate the temperatures (T_b) at which $\epsilon_r(T_b)$ is equal to the energy of the effective impurity level ($\tilde{\epsilon}_d$).

where $\delta \to 0^+$, $\Sigma^U_\sigma(\omega,T)$ is the self-energy due to the Coulomb correlations, and $\Delta_\sigma(\omega)$, given by

$$\Delta_\sigma(\omega) = \int_{-D}^{D} \frac{\Gamma(\omega')/\pi}{(\omega + i\delta) - \omega'} d\omega', \quad (16)$$

is the self-energy caused by the asymmetry of $\Gamma(\omega)$. By expanding both $\Sigma^U_\sigma(\omega,T)$ and $\Delta_\sigma(\omega)$ in powers of ω, $G^f_\sigma(\omega,T)$ can be rewritten as

$$G^f_\sigma(\omega,T) = \frac{z}{(\omega + i\delta) - \epsilon_r(T) - i\mathrm{Im}\tilde{\Delta}_\sigma}, \quad (17)$$

where $z^{-1} = 1 - \mathrm{Re}[\partial\Sigma^U_\sigma(\omega,T)/\partial\omega]_{\omega=0} - [\partial\Delta_\sigma(\omega)/\partial\omega]_{\omega=0}$, $\tilde{\Delta}_\sigma = z\Delta_\sigma(0)$, and $\epsilon_r(T) = z[\epsilon_d + \mathrm{Re}\Sigma^U_\sigma(0,T) + \mathrm{Re}\Delta_\sigma(0)]$ is the energy position of the resonance. Note that the meaning of $\epsilon_r(T)$ differs in the different regimes. In particular, in the FI or LM regime, $\epsilon_r(T)$ is the energy of the effective impurity level $\tilde{\epsilon}_d$, whereas in the SC regime, it is the position of the Kondo resonance.

Figure 4 shows $\epsilon_r(T)$ and $\mathrm{Re}\Sigma^U_\sigma(0,T)$ for different chemical potentials as a function of temperature. As the temperature gets lowered from the high-T VF regime, $\epsilon_r(T)$ would decrease monotonically until the boundary between the VF and FI (LM) regimes for $\mu < 0.0126$ eV ($\mu > 0.0126$ eV) (Fig. 1). At the boundary ($T = T_b$), the impurity level forms and $\epsilon_r(T)$ becomes equal to the energy of the effective impurity level $\tilde{\epsilon}_d$ [i.e., $\tilde{\epsilon}_d = \epsilon_r(T_b)$], as indicated by the arrows in Figs. 2(b) and 4. Clearly, the lowering of $\epsilon_r(T)$ is caused by the decrease of $\mathrm{Re}\Sigma^U_\sigma(0,T)$ due to the increasing strength of the weak interaction between the impurity and conduction electrons [see Fig. 4(a) inset]. Interestingly, at $T = T_b$, $\mathrm{Re}\Sigma^U_\sigma(0,T) \approx -(\epsilon_d + \mu)$ [see Fig. 4(a) inset].

In the case of $\mu < 0.0126$ eV, $\mathrm{Re}\Sigma^U_\sigma(0,T)$ and hence $\epsilon_r(T)$ would then remain unchanged when temperature is further lowered. For very small $|\mu|$ values (e.g., $\mu = 0, \pm 0.001$ eV),

$\tilde{\epsilon_d}$ is located right above the Fermi level [see Fig. 2(b) and Fig. 4(b) inset]. For the negative μ (e.g., $\mu = -0.1$ eV), $\tilde{\epsilon_d}$ would move further above the Fermi level. Therefore, the systems would flow to the FI regime since the impurity state is unbound ($\tilde{\epsilon_d} > 0$). In contrast, for $\mu > 0.0126$ eV (e.g., $\mu = 0.0398$ or 0.1 eV), $\tilde{\epsilon_d} < 0$ and the bound impurity state forms near T_b. Therefore, the system would first flow to the LM regime. As temperature further decreases, the impurity state would then interact very strongly with the conduction electrons, resulting in the pronounced increase of $\mathrm{Re}\Sigma_\sigma^U(0,T)$ [see Fig. 4(a) inset]. Consequently, $\epsilon_r(T)$ would be renormalized to the Fermi level, and the sharp Kondo resonance at the Fermi level would develop [Fig. 3(b)], as the systems move from the LM regime to the SC regime [see Figs. 1(b) and 4]. The local magnetic moment would then be screened at low temperatures. Clearly, $\mu = 0.0126$ eV is the critical μ value that separates the FI and SC regimes [see Fig. 1(b)]. In this case, $\tilde{\epsilon}_d = 0$, i.e., the effective impurity level is located right at the Fermi level.

C. Dephasing rate versus temperature

The calculated dephasing rates as a function of temperature for different chemical potentials are displayed in Fig. 5(a). To help understand the calculated dephasing rates, we show the ω-resolved dephasing rates at zero temperature for different chemical potentials in Fig. 5(b). For the same purpose, we also display the ω-resolved dephasing rates at different temperatures for $\mu = 0.001$ and 0.0398 eV in Fig. 6. The zero-temperature ω-resolved dephasing rates are very similar to the corresponding impurity spectral functions [Fig. 2(b)], except at the Fermi level where the ω-resolved dephasing rates are always zero in the $T = 0$ limit. In general, however, the curves of the dephasing rate as a function of temperature look quite different from that of the resistivity [see Figs. 2(a) and 5(a)]. Figure 5(a) shows that all the dephasing rate curves constitute mainly a prominent peak in the crossover region. When the system enters the crossover region, the dephasing rate increases rapidly as temperature decreases, and reaches the maximum near the center of the crossover region. However, as temperature further decreases, the system enters the SC (FI) regime for $\mu > 0.0126$ eV ($\mu < 0.0126$ eV). Consequently, the dephasing rate drops sharply and finally vanishes in the $T = 0$ limit.

Figure 5(a) shows that, as for the resistivity curves, the dephasing rate curves can be grouped into three cases. In this first case ($\mu < 0.0126$ eV), the dephasing rate curves have a narrower peak compared to that of the conventional Kondo effect. Indeed, the dephasing rate begins to increase at a lower T/T_K than that in normal metals and also in the systems with a large positive μ (e.g., $\mu = 0.0398$ or 0.1 eV). Furthermore, the increasing slope is steep and a fitting to the dephasing rate curve gives a rising function of $\sim 4.6(T_K/T)$. In the lower-temperature side of the peak, the dephasing rate drops more quickly than that in normal metals and also for $\mu \geqslant 0.0126$. A fitting to the dephasing rate curves gives a dropping function of $\sim 0.10(T/T_K)^3$, which is distinctly different from the $(T/T_K)^2$ behavior obtained using Fermi-liquid theory for normal metals [13]. This interesting behavior may be attributed to the fact that the effective impurity

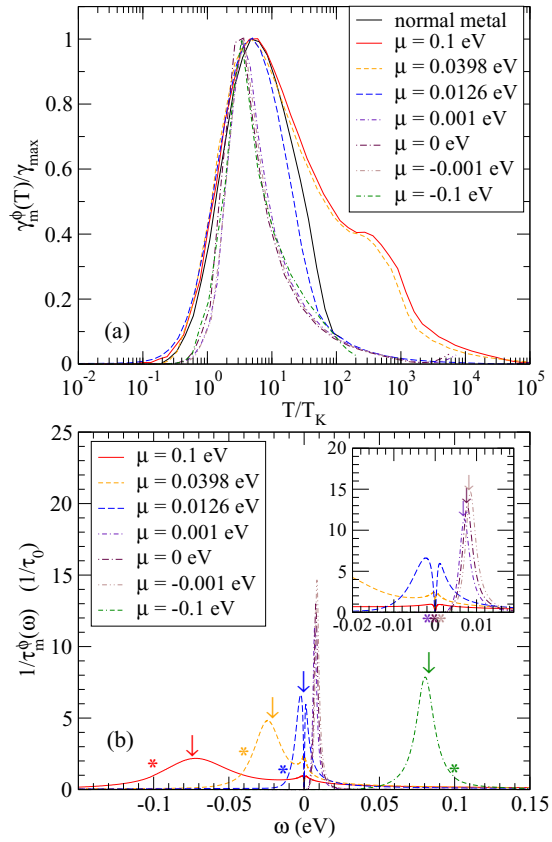

FIG. 5. (Color online) (a) Total dephasing rates as a function of temperature for different chemical potentials. $\gamma_{\max}$ is the maximal dephasing rate. (b) Zero-temperature ω-resolved dephasing rates for different chemical potentials μ. $1/\tau_0 = 2c_{\mathrm{imp}}\hbar v_F^2/\Omega_0|\mu_0|$ with $\mu_0 = 1$ eV. $\omega = 0$ is the Fermi level. The stars indicate the positions of the Dirac point; the arrows denote the positions of the effective impurity level ($\tilde{\epsilon_d}$).

level is located above the Fermi level ($\tilde{\epsilon_d} > 0$) and thus the Fermi level is not in the range of the impurity state peak in the low-T limit [Figs. 2(b), 5(b), and 6(a)]. Therefore, in the crossover from the VF to the FI regime, the dephasing rate, after reaching the maximum, will drop sharply since the width of the peak rapidly becomes narrower with the decreasing temperature [see Fig. 6(a)]. All scatterings, including the inelastic scattering, would be suppressed in the $T = 0$ limit.

In the second case ($\mu > 0.0126$ eV), although the dephasing rate curve is almost identical to the curve of the conventional Kondo effect below the peak temperature (T_m), the dephasing rate curve differs significantly above T_m [Fig. 5(a)]. In particular, the dephasing rate curve has a pronounced shoulder above $100T_K$. This is caused by the occurrence of the LM fixed point in this case (Fig. 1). In the LM regime, the dephasing rate first rises well above $100T_K$ due to the inelastic scattering of the local moment, which gives rise to a broad peak covering the Fermi level [Fig. 5(b)]. This results in a wide shoulder above $100T_K$. In the crossover from the LM to the SC regime, the dephasing rate then rises more quickly to the maximum since the impurity now becomes entangled with the conduction electrons. This is illustrated for $\mu > 0.0398$ eV in the inset in Fig. 6(b), where it is seen that the Kondo

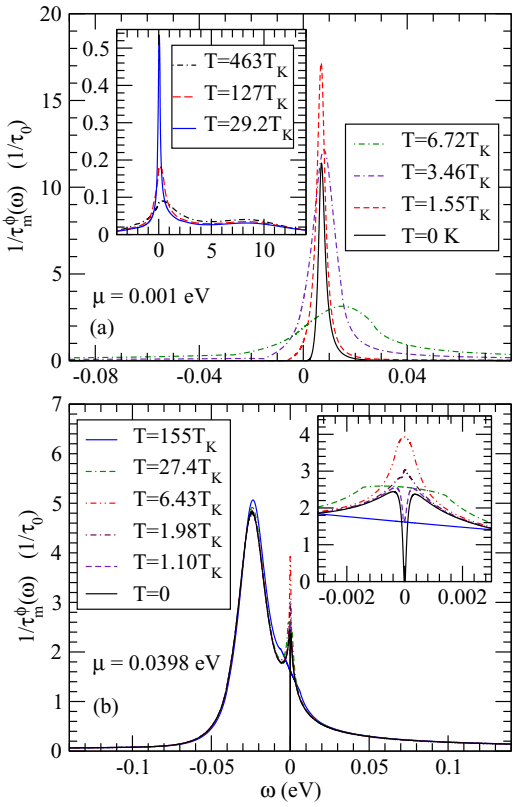

FIG. 6. (Color online) ω-resolved dephasing rates for (a) $\mu = 0.001$ eV and (b) $\mu = 0.0398$ eV at different temperatures. $1/\tau_0 = 2c_{\rm imp}\hbar v_F^2/\Omega_0|\mu_0|$ with $\mu_0 = 1$ eV. $\omega = 0$ is the Fermi level.

resonance grows rapidly as T_K is approached from above. As the temperature further decreases, however, the dephasing rate drops sharply and eventually vanishes because the Kondo resonance starts to decrease and eventually drops to zero [see the inset in Fig. 6(b)] since the impurity magnetic moment is now totally screened.

In the third case (i.e., $\mu \approx 0.0126$ eV), the dephasing rate curve is similar to that for the conventional Kondo effect. In particular, the two dephasing rate curves are nearly identical in the low-temperature side of the peak [Fig. 5(a)]. This is because at this μ value, the Fermi level falls within the range of the impurity state peak in the spectral function [Figs. 2(b) and 5(b)]. This causes the behavior of the dephasing rate to be similar to that of the conventional Kondo effect.

D. Saturation resistivity

As temperature tends to zero, $-[\partial f(\omega)/\partial\omega] \approx \delta(\omega)$, and hence the saturation (i.e., zero-temperature) resistivity can be approximated as

$$\rho_m(0)_{\mu\neq 0} = \frac{\rho_0|V_{\rm hyb}(0)|^2 A_\sigma^f(0,0)}{|\mu|}. \tag{18}$$

For the $\mu = 0$ case, the zero-temperature resistivity should be calculated by using

$$\rho_m(0)_{\mu=0} = \frac{\rho_0|V_{\rm hyb}(0)|^2\Gamma_0/\pi D_{\rm eff}}{\left[\epsilon_d + \Sigma_\sigma^U(0,0)\right]^2}. \tag{19}$$

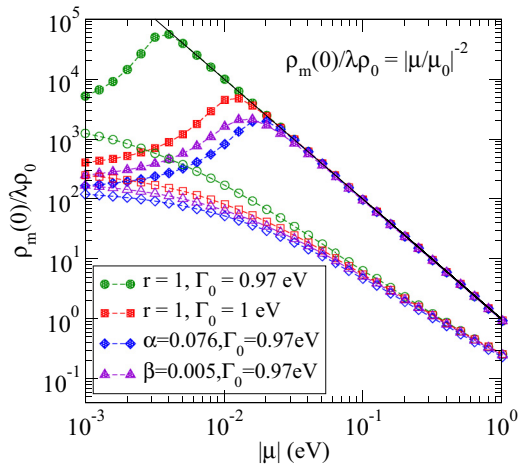

FIG. 7. (Color online) Resistivity at zero temperature as a function of chemical potential. Filled and open symbols are for the positive and negative chemical potentials, respectively. Blue diamond lines are for the case of carbon vacancies, and purple up-triangle lines are for the case of magnetic adatoms.

The calculated zero-temperature resistivity as a function of chemical potential is plotted in Fig. 7. First of all, Fig. 7 shows that the $\rho_m(0)$ values for the negative μ values are more than 10 times smaller than that for the positive μ values, further indicating a strong particle-hole asymmetry in the graphene Kondo systems. This can be explained as follows. For the positive μ values ($\mu > 0.0126$ eV), as discussed in Sec. III B, $\tilde{\epsilon}_d < 0$ and thus the bound impurity state with the local moment is present. Consequently, the system will flow to the SC regime and the Kondo resonance will occur at the Fermi level as temperature goes to zero. This Kondo effect results in a very strong scattering and hence a very large resistivity at $T = 0$ K. For the negative μ values, on the other hand, $\tilde{\epsilon}_d > 0$ and thus the impurity state is unbound. As a result, the system will flow to the FI regime and no Kondo resonance will develop at the Fermi level. Therefore, the scattering will be much suppressed at low temperatures, compared with the case of $\mu > 0.0126$ eV, resulting in a much smaller $T = 0$ resistivity.

Second, Fig. 7 also indicates that for large positive μ values ($\mu > 0.0126$ eV), all of the calculated resistivities at $T = 0$ K collapse onto the solid line determined by Eq. (20). In this case, as mentioned before, the system will flow to the SC regime and $\epsilon_r(T) \approx 0$ at low temperatures. Therefore, $A_\sigma^f(0,0)$ can be approximated as $1/(\pi\Gamma_0\frac{|\mu|}{D_{\rm eff}})$. Plugging this into Eq. (18), the resistivity at $T = 0$ K can be written as

$$\rho_m(0) = \lambda\rho_0\left|\frac{\mu}{\mu_0}\right|^{-2}, \tag{20}$$

where $\lambda = \pi\Omega_0|\mu_0|^2/(4\hbar^2 v_F^2)$ and $\mu_0 = 1$ eV. Clearly, this saturation value is independent of Γ_0, ϵ_d, and U. Therefore, the zero-temperature resistivities collapse onto the solid line determined by Eq. (20). This is also a manifestation of the occurrence of the Kondo resonance in the graphene systems with a positive μ ($\mu \geqslant 0.0126$ eV).

E. Effect of higher-order terms

Finally, we consider the first higher-order term. Figure 7 shows that the results for the cases of $\alpha \neq 0$ and $\beta \neq 0$ qualitatively agree with the case of the pure power law of $r = 1$, albeit with a larger Γ_0. This is because for the case of carbon vacancies, total hybridization becomes larger when the higher-order terms are considered, resulting in a larger effective Γ_0. For the case of magnetic adatoms, in the presence of the hybridization between the impurity and the conduction electrons on the next-nearest neighbors, $\Gamma(\omega)$ becomes asymmetric, giving rise to a larger $\mathrm{Re}\Delta_\sigma(0)$. Therefore, the effective impurity level will rise. As a result, the system needs a larger chemical potential to bring the effective impurity level back to below the Fermi level, which has the same effect of a larger Γ_0.

IV. COMPARISON TO EXPERIMENTS

Recent experiments showed that the Kondo effect could be observed in graphene with point defects and vacancies [22]. Two prominent features about the transport properties from the experiments were reported [22]. First, the Kondo effect was observed in graphene under a wide range of applied gate voltages (up to $|V_g| = \sim 50$ V, which is equivalent to $|\mu| = \sim 0.25$ eV). Second, the normalized Kondo part of the resistivity appeared to be a universal function of $T/T_K(V_g)$, which could fit well to that for the conventional Kondo effect obtained from much earlier NRG calculations [32]. In principle, this could be explained as follows. With a large applied gate voltage, the Dirac point would lie well below the Fermi level. The two important properties of graphene, namely, zero density of states at the Dirac point and linear energy dependence of the density of states, would hardly affect the transport properties of the system. Therefore, the system would behave like the conventional Kondo system. Indeed, as discussed before in Sec. III A, the shape of the resistivity-versus-T curve for $\mu \approx 0.0126$ eV calculated here looks very similar to that of the conventional Kondo effect [Fig. 2(a)]. However, as reported in Sec. III A, our calculated resistivity curves for other chemical potentials show several unusual features which were not observed in the experiments [22].

Very recently, the difficulties in uncovering the Kondo effect in graphene by resistivity measurements because of a possible similar contribution from the electron-electron interaction to the low-temperature resistivity were reported [39]. On the other hand, Fig. 5(a) shows that all of the dephasing rates in the graphene Kondo systems exhibit characteristic features that are distinctly different from that of the conventional Kondo effect. Therefore, we would suggest further measurements on the dephasing rate in graphene. With the distinct characteristics we have shown in Sec. III, the unusual features of the resistivity and dephasing rate in graphene could be identified. Furthermore, we would also suggest further scanning tunneling spectroscopy (STS) experiments on the Kondo effect in graphene. As noted in Sec. III A, in the FI regime, the impurity spectral function has only one peak at the effective impurity level above the Fermi level. On the other hand, in the SC regime, the spectral function has two peaks, located at the Fermi level and also at the effective impurity level below the Fermi level, respectively. These spectroscopic signatures of the FI and SC regimes could be used in future STS experiments to differentiate whether the "Kondo effect" in graphene takes place from the VF to the FI regime or from the LM to the SC regime.

V. CONCLUSIONS

We have investigated the resistivity and dephasing rate in the Kondo regime due to magnetic impurities in graphene under different gate voltages by NRG calculations. We find that although the Anderson impurity model considered here is a mixed-valence system, it can be driven into either the Kondo [$\mu > \mu_c$], mixed-valency ($\mu \approx \mu_c$), or empty-orbital ($\mu < \mu_c$) regime by a gate voltage, thereby resulting in characteristic features in resistivity and dephasing rate in each regime. In particular, in the case of $\mu < \mu_c$, the shapes of the resistivity (dephasing rate) curves are nearly identical. However, as temperature decreases, they start to increase to their maxima at a lower T/T_K, but more rapidly [as $(T_K/T)^{3/2}$] than in normal metals. As T further decreases, after reaching the maximum, the dephasing rate drops more quickly than in normal metals, behaving as $(T/T_K)^3$ instead of $(T/T_K)^2$. Furthermore, the resistivity has a pronounced peak above the saturation value near T_K. In the case of $\mu > \mu_c$, in contrast, the resistivity curve has an additional broad shoulder above $10T_K$ and the dephasing rate exhibits an interesting shoulder-peak shape. In the narrow boundary region ($\mu \approx \mu_c$), both the resistivity and dephasing rate curves are similar to the corresponding ones in normal metals. The interesting results of the resistivity and dephasing rate are analyzed in terms of the calculated spectral function, self-energy due to Coulomb correlation, and also effective impurity level. The calculated resistivity in the vicinity of $\mu \approx \mu_c$ is in good agreement with the conventional Kondo-like resistivity observed in the recent experiments, although the interesting features in the resistivity in the other cases ($\mu < \mu_c$ or $\mu > \mu_c$) predicted here were not seen in the experiments. We hope that the unusual features of the Kondo resistivity and dephasing rate in graphene reported here will stimulate further transport experiments on the Kondo effect in graphene.

ACKNOWLEDGMENTS

The authors thank Ya-Fen Hsu, Chung-Han Wang, and Jong-Chin Lin for fruitful discussions. Financial support for this work from the National Science Council, the Academia Sinica Thematic Research Program, and the National Center for Theoretical Sciences of Taiwan as well as the Deutsche Forschungsgemeinschaft under Grant No. AN 275/7 is gratefully acknowledged.

[1] K. S. Novoselov, A. K. Geim, S. V. Morozov, D. Jiang, Y. Zhang, S. V. Dubonos, I. V. Grigorieva, and A. A. Firsov, Science **306**, 666 (2004).

[2] K. S. Novoselov, A. K. Geim, S. V. Morozov, D. Jiang, M. I. Katsnelson, I. V. Grigorieva, S. V. Dubonos, and A. A. Firsov, Nature (London) **438**, 197 (2005).

[3] A. H. Castro Neto, F. Guinea, N. M. R. Peres, K. S. Novoselov, and A. K. Geim, Rev. Mod. Phys. **81**, 109 (2009).
[4] L. Fritz and M. Vojta, Rep. Prog. Phys. **76**, 032501 (2013).
[5] O. V. Yazyev and L. Helm, Phys. Rev. B **75**, 125408 (2007).
[6] K. T. Chan, J. B. Neaton, and M. L. Cohen, Phys. Rev. B **77**, 235430 (2008).
[7] B. Uchoa, V. N. Kotov, N. M. R. Peres, and A. H. Castro Neto, Phys. Rev. Lett. **101**, 026805 (2008).
[8] T. O. Wehling, A. V. Balatsky, M. I. Katsnelson, A. I. Lichtenstein, and A. Rosch, Phys. Rev. B **81**, 115427 (2010).
[9] T. O. Wehling, A. I. Lichtenstein, and M. I. Katsnelson, Phys. Rev. B **84**, 235110 (2011).
[10] J. O. Sofo, G. Usaj, P. S. Cornaglia, A. M. Suarez, A. D. Hernández-Nieves, and C. A. Balseiro, Phys. Rev. B **85**, 115405 (2012).
[11] R. R. Nair, M. Sepioni, I. L. Tsai, O. Lehtinen, J. Keinonen, A. V. Krasheninnikov, T. Thomson, A. K. Geim, and I. V. Grigorieva, Nat. Phys. **8**, 199 (2012).
[12] P. W. Anderson, Phys. Rev. **124**, 41 (1961).
[13] A. C. Hewson, *The Kondo Problem to Heavy Fermions* (Cambridge University Press, Cambridge, 1993).
[14] D. Withoff and E. Fradkin, Phys. Rev. Lett. **64**, 1835 (1990).
[15] K. Chen and C. Jayaprakash, J. Phys.: Condens. Matter **7**, L491 (1995).
[16] K. Ingersent, Phys. Rev. B **54**, 11936 (1996).
[17] R. Bulla, T. Pruschke, and A. C. Hewson, J. Phys.: Condens. Matter **9**, 10463 (1995).
[18] C. Gonzalez-Buxton and K. Ingersent, Phys. Rev. B **57**, 14254 (1998).
[19] L. Fritz and M. Vojta, Phys. Rev. B **70**, 214427 (2004).
[20] M. Cheng and K. Ingersent, Phys. Rev. B **87**, 075145 (2013).
[21] T. Kanao, H. Matsuura, and M. Ogata, J. Phys. Soc. Jpn. **81**, 063709 (2012).
[22] J. H. Chen, L. Li, W. G. Cullen, E. D. Williams, and M. S. Fuhrer, Nat. Phys. **7**, 535 (2011).
[23] K. Sengupta and G. Baskaran, Phys. Rev. B **77**, 045417 (2008).
[24] H. B. Zhuang, Q. F. Sun, and X. C. Xie, Europhys. Lett. **86**, 58004 (2009).
[25] M. Vojta, L. Fritz, and R. Bulla, Europhys. Lett. **90**, 27006 (2010).
[26] P. S. Cornaglia, G. Usaj, and C. A. Balseiro, Phys. Rev. Lett. **102**, 046801 (2009).
[27] D. Jacob and G. Kotliar, Phys. Rev. B **82**, 085423 (2010).
[28] K. G. Wilson, Rev. Mod. Phys. **47**, 773 (1975).
[29] Z. G. Zhu, K. H. Ding, and J. Berakdar, Europhys. Lett. **90**, 67001 (2010).
[30] B. Uchoa, T. G. Rappoport, and A. H. Castro Neto, Phys. Rev. Lett. **106**, 016801 (2011).
[31] H. R. Krishna-murthy, J. W. Wilkins, and K. G. Wilson, Phys. Rev. B **21**, 1044 (1980).
[32] T. A. Costi, A. C. Hewson, and V. Zlatic, J. Phys.: Condens. Matter **6**, 2519 (1994).
[33] R. Bulla, A. C. Hewson, and T. Pruschke, J. Phys.: Condens. Matter **10**, 8365 (1998).
[34] G. Zaránd, L. Borda, J. von Delft, and N. Andrei, Phys. Rev. Lett. **93**, 107204 (2004).
[35] B. L. Altshuler and A. G. Aronov, *Electron-Electron Interaction in Disordered Systems* (North-Holland, Amsterdam, 1985).
[36] T. Micklitz, A. Altland, T. A. Costi, and A. Rosch, Phys. Rev. Lett. **96**, 226601 (2006).
[37] E. J. Nicol and J. P. Carbotte, Phys. Rev. B **80**, 081415 (2009).
[38] The resistivity for the normal-metal Kondo system is calculated by assuming the scattering rate $\Gamma(\omega)$ is constant [i.e., $\Gamma(\omega) = \Gamma_0$]. The impurity level $\epsilon_d = -1.5$ eV used is determined by letting its occupation number (n) be approximately equal to that in the graphene system with $\mu = 0.1$ eV [see the inset in Fig. 2(a)]. The other parameters are the same as in the graphene case, i.e., $\Gamma_0 = 1$, $U = 10$, and $D = 20$ eV.
[39] J. Jobst, F. Kisslinger, and H. B. Weber, Phys. Rev. B **88**, 155412 (2013).